Supplementary Material

1 Simulated systems

In tables 1 to 5, the exact compositions and system sizes (cubic box length) are given for all simulations performed for this study. The simulation times for the different systems at the production temperatures ranging from $T = 380$ K to $T = 270$ K are given in table 6. The randomization and pre-equilibration at the elevated temperatures $T = 500$, 450 and 400 K have been performed for 1, 2, 3, 4 and 5 ns at each temperature for glucose, maltose, maltotriose, maltotetraose and maltopentose sysetms respectively. For maltotriose, a slightly different temperature scheme has been used as well. For the glucose water-mixtures, a few additional runs in the temperature range between $T = 370$ K and $T = 450$ K have been performed which have been used in the analysis of the rotational autocorrelation function.

Fast annealing simulations: In addition to these simulations a larger number of fast annealing simulations have been performed at 90 wt. % in order to get a better estimate for the free volume at this maltooligomer concentration. For this the systems have been simulated for 5 ns at $T = 500$ K in order to produce 20 independent start configurations for each system (simulation time distance 250 ps at $T = 500$ K). Each starting configuration was then annealed during 5 ns from $T = 500$ K to $T = 250K$. The last frame of the 300 ps simulation runs at each temperature have been used for the analysis.

Additional long and large simulations: In table 7 the details of some 100 ns simulations and a large simulation with a box size of 5.81 nm are given. The long simulation runs have been started from the last frame of the corresponding normal simulation runs (No. 1 to 53 in tables 1 to 5) at the given concentration and temperature.

2 Comparison with long runs and finite size effects

Long Runs: Additional long simulation runs of 100 ns have been performed for selected systems at specific temperatures. Details of these systems can be found in table 7. The 100 ns simulation runs can be divided in two groups. The larger group (No. 54,55,56,58 and 60) are located in or close to the equilibrated region whereas the second group (No. 57 and 59) are well in the non-equilibrated glassy region. In figures 1 to 4 we show the evolution of the radial distribution function (RDF) of water oxygens and the mean square displacement (MSD) of water molecules with simulation time for three of our long run simulations. The first one, a 60 wt.% maltopentose content at $T = 350$ K, is placed on the edge of the equilibrated region. No differences between the initial 10 ns and the final 10 ns can be seen for both the water oxygen RDF (fig. 1) and the water MSD (fig. 2). The second case is a simulation at 90 wt.% glucose content at $T = 350$ K. In this case the MSD of the glucose molecules is 0.1 nm^2 after 2 ns and

1.8 nm^2 after 100 ns. This means we consider the glucose translational mobility to be frozen in on a ns scale whereas for a 100 ns scale the glucose molecule must be considered mobile. Also in this case we do not see significant aging during the long simulation run as can be seen by the comparison between the inital and final 10 ns shown for the water oxygen RDF in fig. 3 and for the water MSD in fig. 4. A slightly different situation can be found in the third case, a simulation at 90 wt.% maltotriose content at $T = 350$ K. Here even after 100 ns the MSD of the maltotriose molecule is smaller than 0.25 nm^2, so we consider it as a frozen-in molecule. Some aging effects are visible in the RDF of water oxygens. This is shown in fig. 5. As indicated in the figure, the final distribution of water oxygens is reached after 50 ns. A similar aging can also be observed in other RDFs of the same system (results not shown). This also has some effects on dynamic quantities, but the effect here is not as clear as for the RDF. The reason for this is the limited accuracy with which we can measure the MSD of water molecules in this region. The results for the MSD of water are shown in fig. 6. In particular, no unique trend in the water MSD with respect to the aging is observed. We therefore are convinced that the observed aging effects, if at all present in the much shorter production runs, do not affect our results and conclusions.

Finite size effects: In order to investigate possible finite size effects we simulated a larger analog of a 60 wt. % glucose water mixture. The standard or 'normal' simulation (no. 6 in table 1) contains 55 glucose molecules, whereas the large simulation (no. 61 in table 7) contains 500 glucose molecules and 3205 water molecules giving rise to a box size of 5.81 nm^3. The density, showing a deviation of 0.3 %, and the diffusion constants for water and glucose, showing a difference of 5 %, are well within the error bars for these quantities. To show that there is no significant difference in structural properties fig. 7 shows a comparison of the mixed RDF between carbohydrate oxygens (O_c)and water oxygens (O_w) between the two simulations.

3 Validation: Densities and Diffusion Coefficients

For glucose and maltose water mixtures we could find density data over a wide range of concentrations in the literature [1, 2]. In addition we have density measurements on maltose water mixtures in the low water content regime from our own laboratory. A comparison between the experimental and the simulated data is shown in fig. 8 and shows excellent agreement. Here one has to keep in mind that density data from atomistic simulations is expected to have an accuracy of roughly 1%. In fig. 8 the data for maltose water mixtures is shifted upwards by 100 g/l for clarity.

The experimental data on diffusion coefficients of both water and maltooligomers in mixtures is rather sparse. The comparison with our simulations which is shown for water diffusion in fig. 9 and for glucose diffusion in fig. 10 is based on experimental data from refs. [3, 4]. The study of Moran and Jeffrey [3] is based on NMR experiments, whereas the study of Talon et

al. [4] has been performed with help of quasi elastic neutron scattering (QENS). For the water diffusion coefficient we find good agreement for both 15 and 75 wt.% glucose content with a slight tendency for values which are on the high side in the simulations. For 48 wt.% the water diffusion coefficient calculated from the simulations is a factor two larger then the experimental values. A prediction of diffusion coefficients from atomistic simulations within a factor of two is well accepted in the field and is still considered as a good agreement. Here we want to remark that also the experimental determination of diffusion coefficients also exhibits a rather large uncertainty and depends on the experimental method and on the theoretical model for the data interpretations. For example the experimental values for the water diffusion coefficient at T = 280 K at a glucose content of 48 wt.% obtained in two different QENS studies [5, 4] using two different theoretical models differ by more than a factor of 10. Further validation of the force field can be deduced from the slopes of the temperature dependence of the diffusion coefficients shown in fig. 9 and fig. 10 which are quite similar between the experimental studies and the results from our simulations. This means that the activation energies for the diffusion processes can be predicted by the simulations with good accuracy.
We conclude that the simulations with the used force field are overall in good agreement with experimental findings for both static and dynamic properties. In addition, we find that the force field is valid over a reasonably wide range of temperatures and concentrations.

4 Comparison with fixed $^4C_1$ chair conformations

Due to the large fraction of non-chair conformations found in the simulations we performed additional simulations where we fixed the $^4\mathrm{C}_1$ chair conformer of the glucose heterocycle with help of additional dihedral potentials at the ring atoms. These simulations with fixed rings (FR) for glucose water mixtures follow exactly the same setup and simulation procedure as the normal (N) glucose-water mixture simulations (see table 1 and 6 for the exact compositions and simulation times).
In fig. 11 the densities of the glucose water mixtures at $T = 310$ K are compared between FR and N simulations. Exept for 100 wt.% glucose content no difference can be detected. The difference at 100 wt.% is in the range of the usual uncertainty at this maltooligomer content. Also for the water oxygen RDF we can not see any difference as is apparent from fig. 12. Only for RDFs where atoms in the glucose molecules are involved directly show some differences between FR and N simulations. As can be seen for the mixed RDF between glucose and water oxygens shown in fig. 13 and for the glucose oxygen RDF shown in fig 14 the differences only become significant at very high glucose concentrations. Since there is a change in the conformation of the glucose molecules these differences are logical. However we want to remark that the difference indicated with an arrow at $r = 0.53$ nm in fig. 13 does not change our interpretation of figure 9 in the main article, where we compare the mixed RDF between glucose and water

oxygens with the intermolecular RDF for oxygen molecules.
We also tested the implications of this slight difference in the static ordering between the atoms on the dynamic properties. In fig. 15 the MSD for water molecules is compared for 40, 70 and 90 wt.% glucose content between N (blue) and FR (red) simulations. For 40 wt.% we also performed three independent runs (only difference here is the initial system setup) in order to estimate the uncertainty of the observed quantity. The differences between N and FR simulations are very small, do not show a trend in any direction and are well within the uncertainty of the MSD. The same argumentation can also be made for the MSD of glucose molecules in the same systems which is shown in fig. 16.
From this detailed comparison, we conclude that the overestimation of non chair conformers present in the OPLS force field does not affect our results and conclusions. However, we think that the discrepancy should be considered in the development of the next generation of carbohydrate force fields in agreement with the conclusions drawn in a recent study of the GROMOS 45a5 force field [6].

References

[1] C. A. Cerderiña, E. Carballo, C. A. Tovar and L. Romani, *J. Chem. Eng. Data*, 1997, **42**, 124–127.

[2] D. Lourdin, P. Colonna and G. Ring, *Carbohydr. Res.*, 2003, **338**(24), 2883–2887.

[3] G. R. Moran and K. R. Jeffrey, *J. Chem. Phys.*, 1999, **110**, 3472.

[4] U. Talon, L. J. Smith, J. W. Brady, B. A. Lewis, J. R. D. Copley, D. L. Price and M. L. Saboungi, *J. Phys. Chem. B*, 2004, **108**(16), 5120–5126.

[5] L. J. Smith, D. L. Price, Z. Chowdhuri, J. W. Brady and M. L. Saboungi, *J. Chem. Phys.*, 2004, **120**(8), 3527–3530.

[6] V. Krautler, M. Muller and P. H. Hünenberger, *Carbohydr. Res.*, 2007, **342**(14), 2097–2124.

Table 1: Glucose-water mixtures. Concentration is given in wt. % malto oligomer (MO). The third and fourth column give the number of molecules for MO and H_2O. Box size is given for $T = 310$ K

No.	Conc. Wt. %	MO #	H_2O #	Box nm
1	10	8	726	2.86
2	20	16	638	2.81
3	30	25	569	2.80
4	40	35	519	2.81
5	50	45	445	2.80
6	60	55	359	2.77
7	70	70	299	2.82
8	80	85	212	2.83
9	85	95	169	2.87
10	90	110	121	2.94
11	95	120	63	2.96
12	100	130	0	2.97

Table 2: Maltose-water mixtures. Concentration is given in wt. % malto oligomer (MO). The third and fourth column give the number of molecules for MO and H_2O. Box size is given for $T = 310$ K

No.	Conc. Wt. %	MO #	H_2O #	Box nm
13	10	8	1389	3.53
14	20	15	1145	3.41
15	30	20	855	3.20
16	40	25	710	3.11
17	50	30	548	3.00
18	60	35	491	3.01
19	70	40	328	-
20	80	40	190	2.77
21	85	50	167	2.85
22	90	40	82	2.58
23	95	40	40	2.52
24	100	40	0	2.48

Table 3: Maltotriose-water mixtures. Concentration is given in wt. % malto oligomer (MO). The third and fourth column give the number of molecules for MO and H_2O. Box size is given for $T = 300$ K

No.	Conc. Wt. %	MO #	H_2O #	Box nm
25	10	6	1498	3.64
26	20	8	893	3.14
27	30	10	651	2.91
28	40	15	632	2.99
29	50	20	560	3.00
30	60	25	467	3.00
31	70	30	360	2.98
32	80	30	210	2.80
33	90	30	93	2.68
34	100	30	0	2.57

Table 4: Maltotetraose-water mixtures. Concentration is given in wt. % malto oligomer (MO). The third and fourth column give the number of molecules for MO and H_2O. Box size is given for $T = 310$ K

No.	Conc. Wt. %	MO #	H_2O #	Box nm
35	10	3	1006	3.19
36	20	5	736	2.95
37	30	7	606	2.84
38	40	10	553	2.86
39	50	13	484	2.86
40	60	17	419	2.91
41	70	21	333	2.93
42	80	25	231	2.93
43	90	30	123	2.94
44	100	35	0	3.06

Table 5: Maltopentose-water mixtures. Concentration is given in wt. % malto oligomer (MO). The third and fourth column give the number of molecules for MO and H_2O. Box size is given for $T = 310$ K

No.	Conc. Wt. %	MO #	H_2O #	Box nm
45	20	5	909	3.16
46	30	8	844	3.18
47	40	10	686	3.08
48	50	15	710	3.24
49	60	20	713	3.38
50	70	25	493	3.31
51	80	25	288	3.12
52	90	25	128	2.96
53	100	25	0	2.86

Table 6: Simulation times for the different systems. Temperatures are given in K. For maltotriose a slightly different temperature scheme has been used. [a]: only for 40 to 80 wt. %

MO type / Temp.	370	350	330	310	190	270
Glucose	2	2	3	4	5	6
Maltose	-	2	4	4	4	4
Maltotetraose	3	3	4	5	6	5[a]
Maltopentose	4	5	6	7	3	3
	380	360	350	340	320	300
Maltotriose	3 3	3	3	3	3	3

Table 7: Additional long or large simulations. System sizes are as for the other simulations except No. 61 which contains 500 glucose and 3205 water molecules.

No.	MO type	conc. wt. %	Box nm	T K	time ns
54	gluc.	60	2.78	330	100
55	gluc.	90	2.95	350	100
56	malt.	60	3.02	330	100
57	malt.	90	2.59	350	100
58	trio.	60	3.01	330	100
59	trio.	90	2.69	350	100
60	pent.	60	3.40	350	100
61	gluc.	60	5.81	350	10

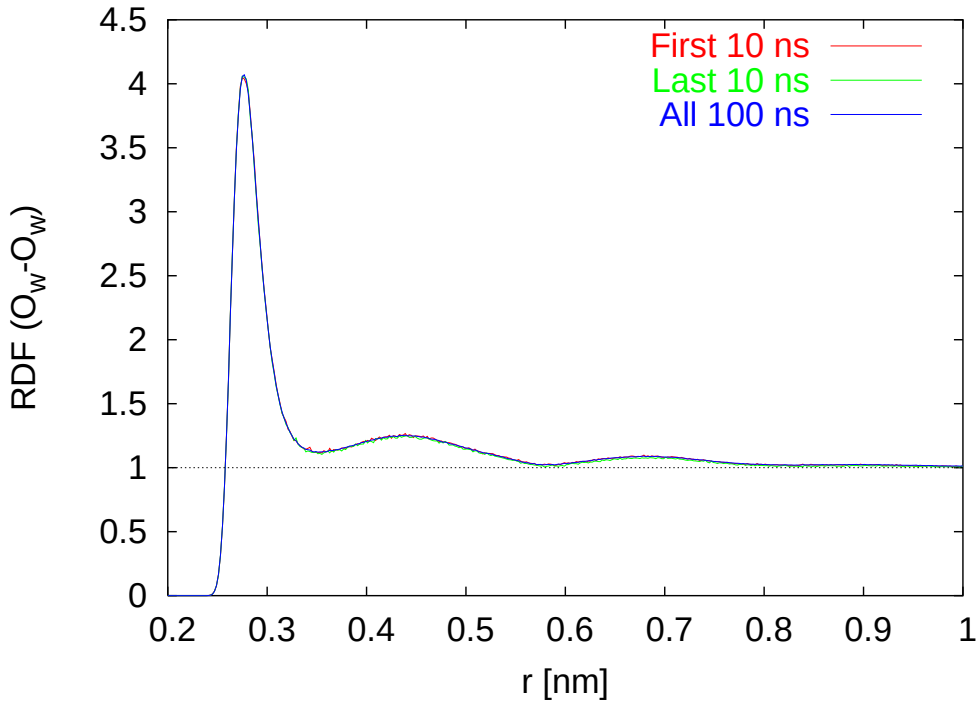

Figure 1: Comparison of the RDF of water oxygens (O_w) at the beginning and the end of a 100 ns simulation run of a 60 wt.% maltopentose content at $T = 350$ K .

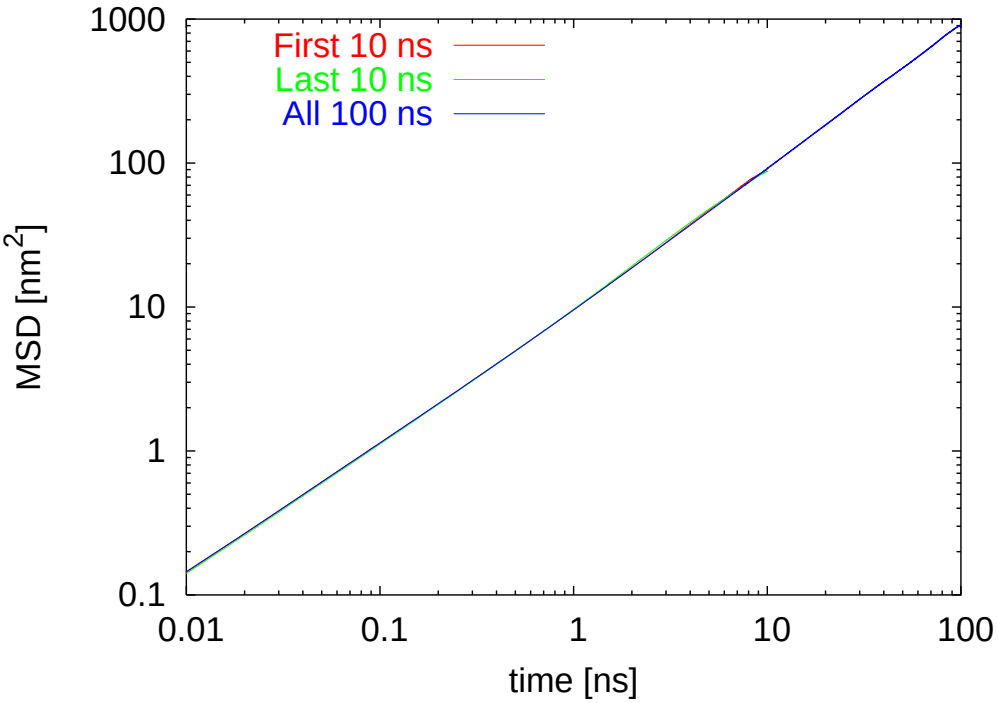

Figure 2: Comparison of the MSD of water molecules at the beginning and the end of a 100 ns simulation run of a 60 wt.% maltopentose content at $T = 350$ K.

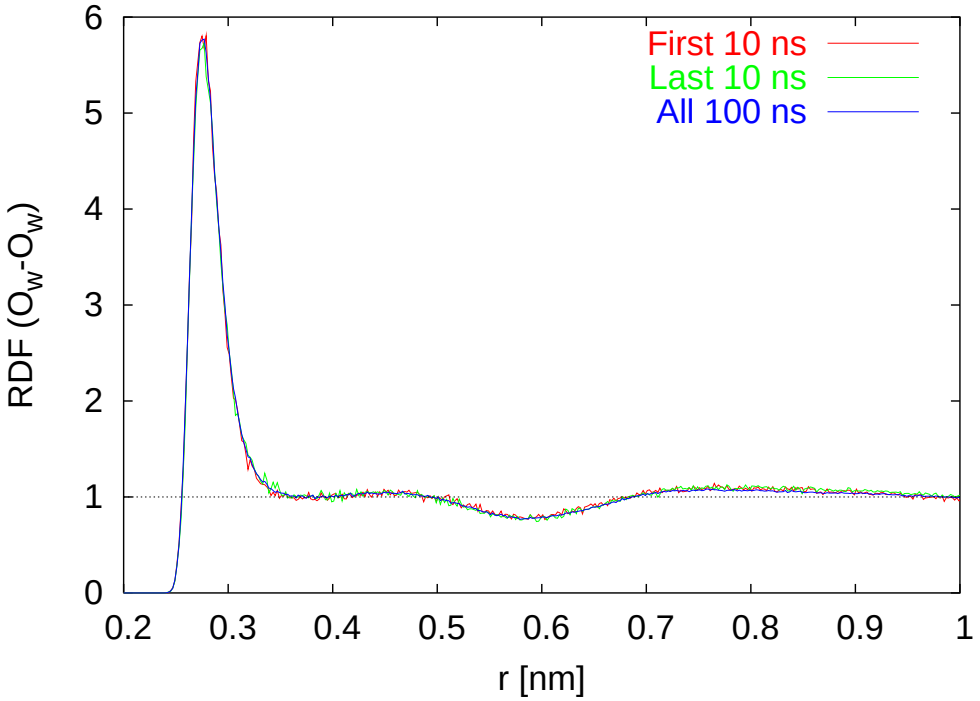

Figure 3: Comparison of the RDF of water oxygens (O_w) at the beginning and the end of a 100 ns simulation run of a 90 wt.% glucose content at $T = 350$ K.

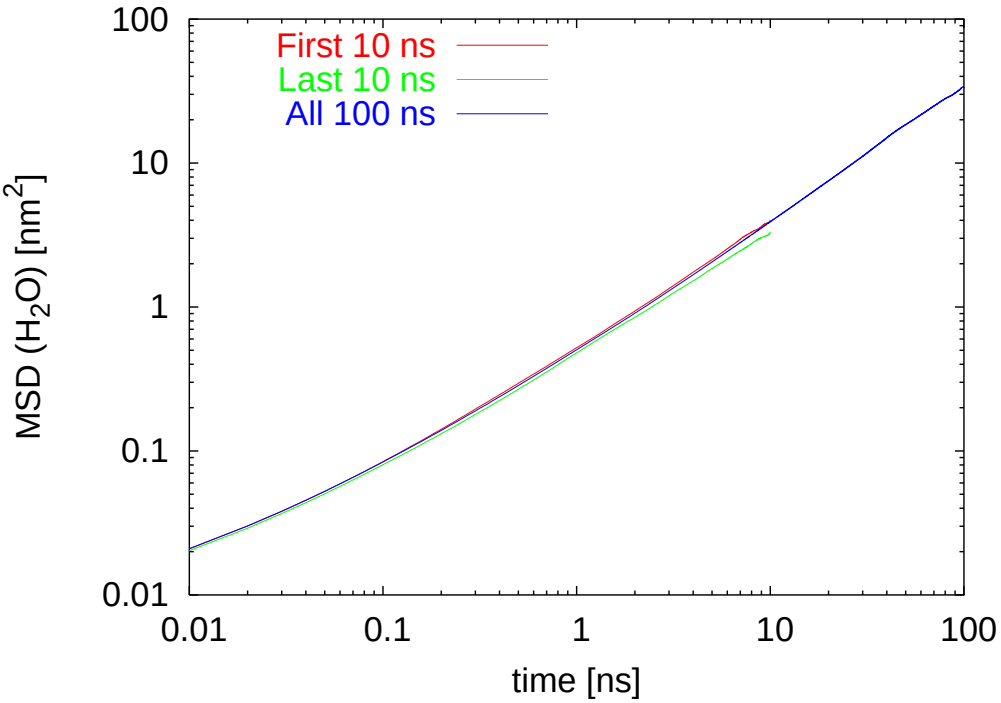

Figure 4: Comparison of the MSD of water molecules at the beginning and the end of a 100 ns simulation run of a 90 wt.% glucose content at $T = 350$ K.

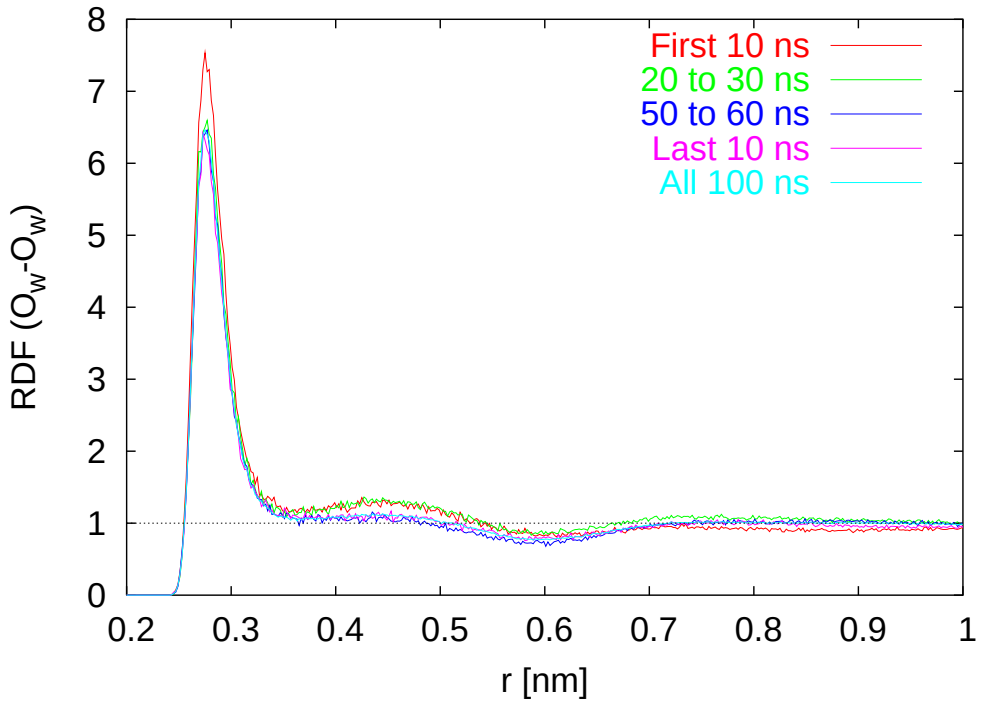

Figure 5: Comparison of the RDF of water oxygens (O_w) at the beginning and the end of a 100 ns simulation run of a 90 wt.% maltotriose content at $T = 350$ K.

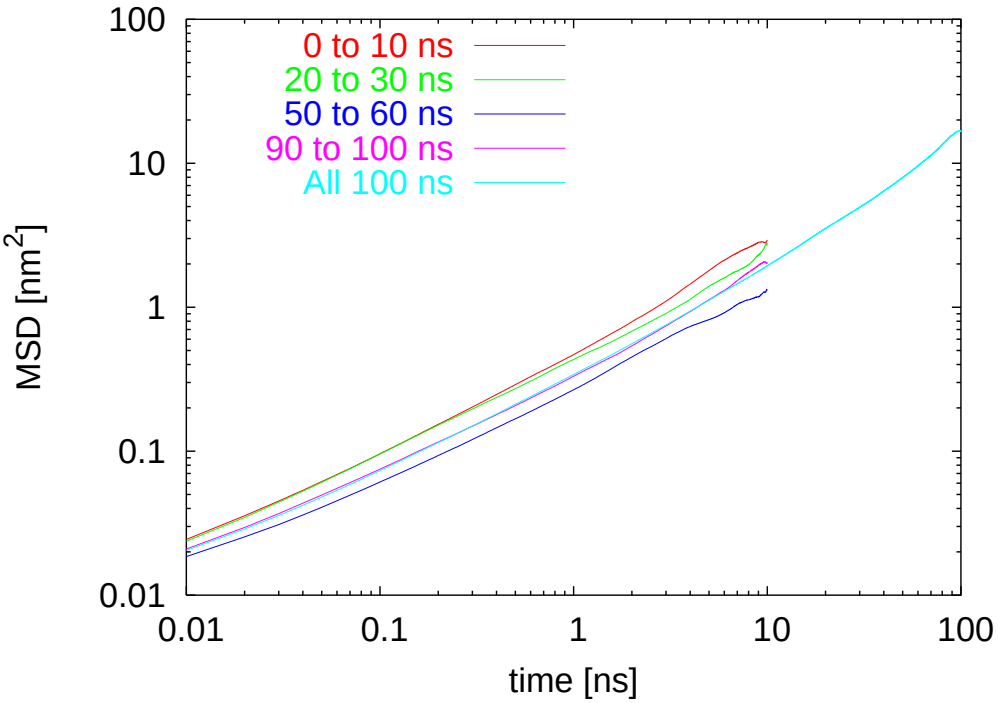

Figure 6: Comparison of the MSD of water molecules at the beginning and the end of a 100 ns simulation run of a 90 wt.% maltotriose content at $T = 350$ K.

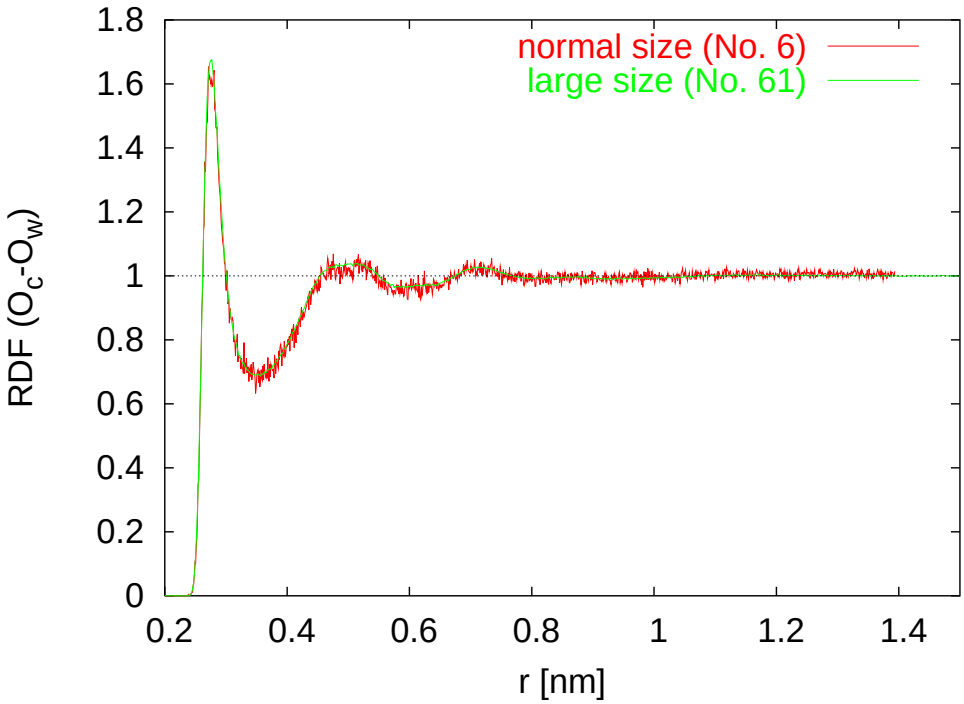

Figure 7: Comparison of the mixed RDF between carbohydrate oxygens (O_c)and water oxygens (O_w) at $T = 350$ K between two simulations with different box size: Normal size (No. 6): box size 2.79 nm; Large size (No. 61): box size 5.81 nm.

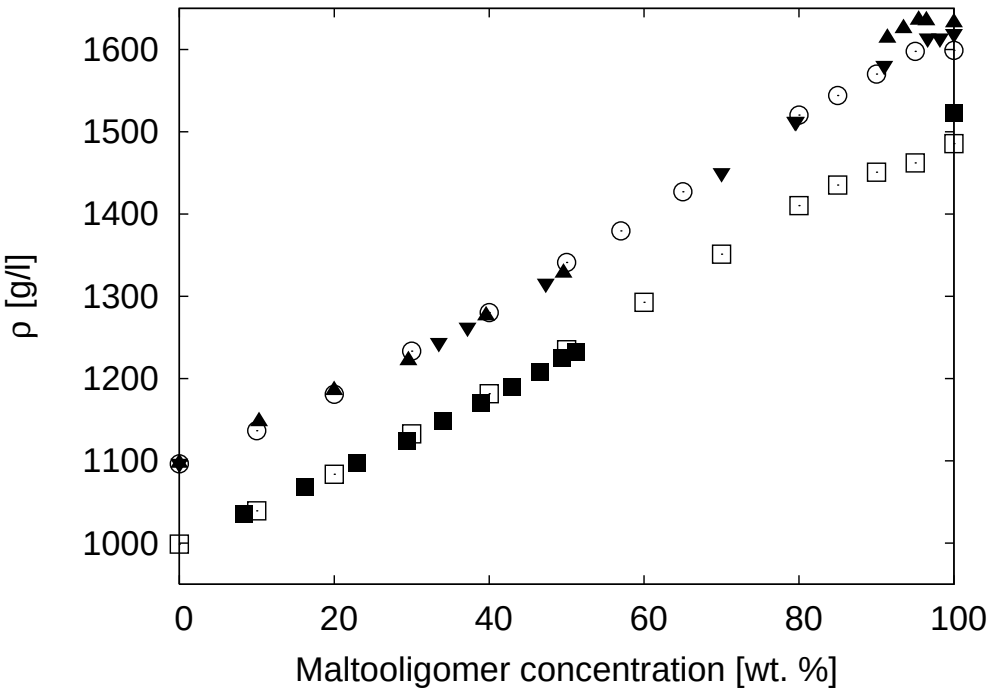

Figure 8: Comparison of experimental and simulated densities for glucose and maltose water mixtures at room temperature. The data for maltose is shifted upwards by 100 g/l for clarity. □ - simulated glucose-water mixtures; ■ - experimental glucose-water mixtures [1]; ○ - simulated maltose-water mixtures; ▲ - experimental maltose-water mixtures [2]; ▼ - experimental maltose-water mixtures (own data).

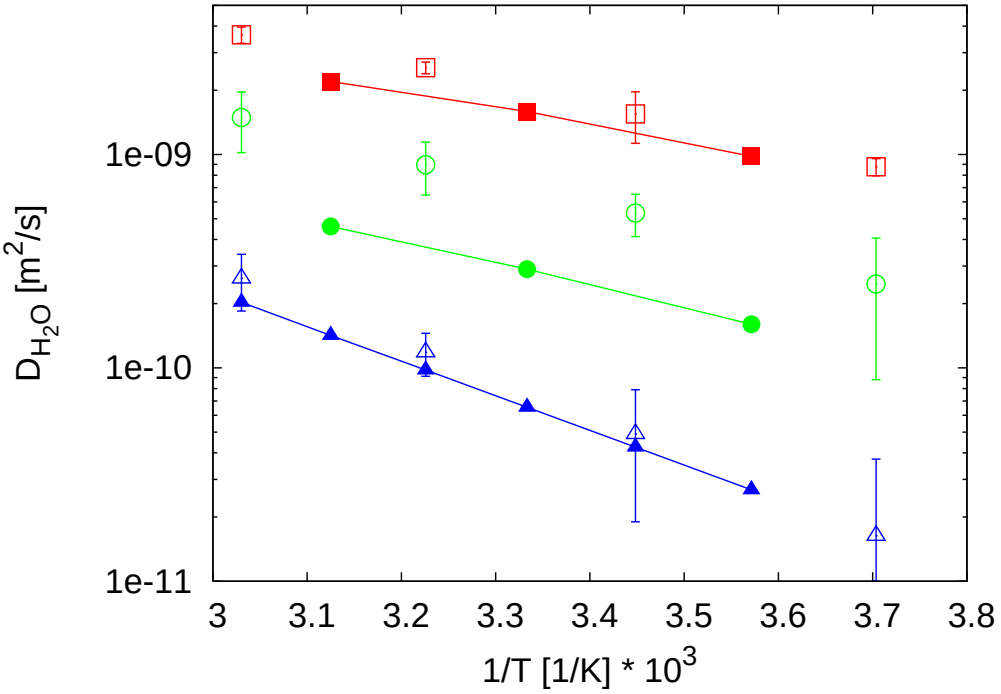

Figure 9: Comparison of experimental and simulated H_2O diffusion coefficients for glucose water mixtures at differnt glucose contents given in wt.%. □ - simulations 15 wt.% (average between simulations at 10 and 20 wt.%) ■ - experiments 15 wt.% [4]; ○ - simulations 50 wt.%; ● - experiments 48 wt.% [3]; △ - simulation 75 wt.% (average between simulations at 70 and 80 wt.%); ▲ - experiments 75 wt.% [3].

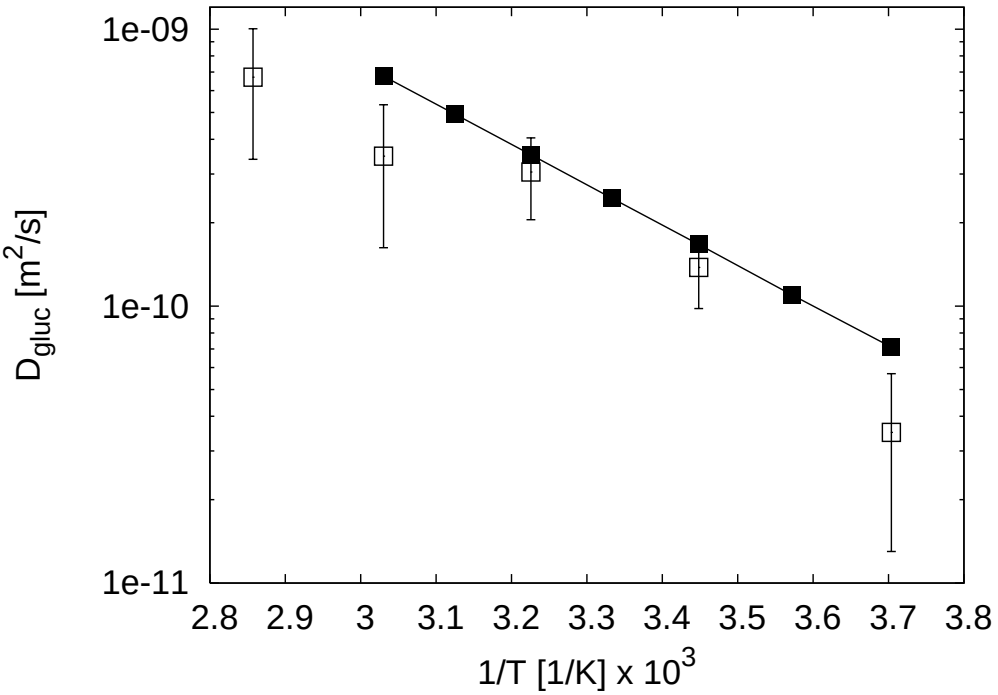

Figure 10: Comparison of experimental and simulated glucose diffusion coefficients for glucose-water mixtures at 40 wt.% glucose content. □ - simulations; ■ - experimental values [3].

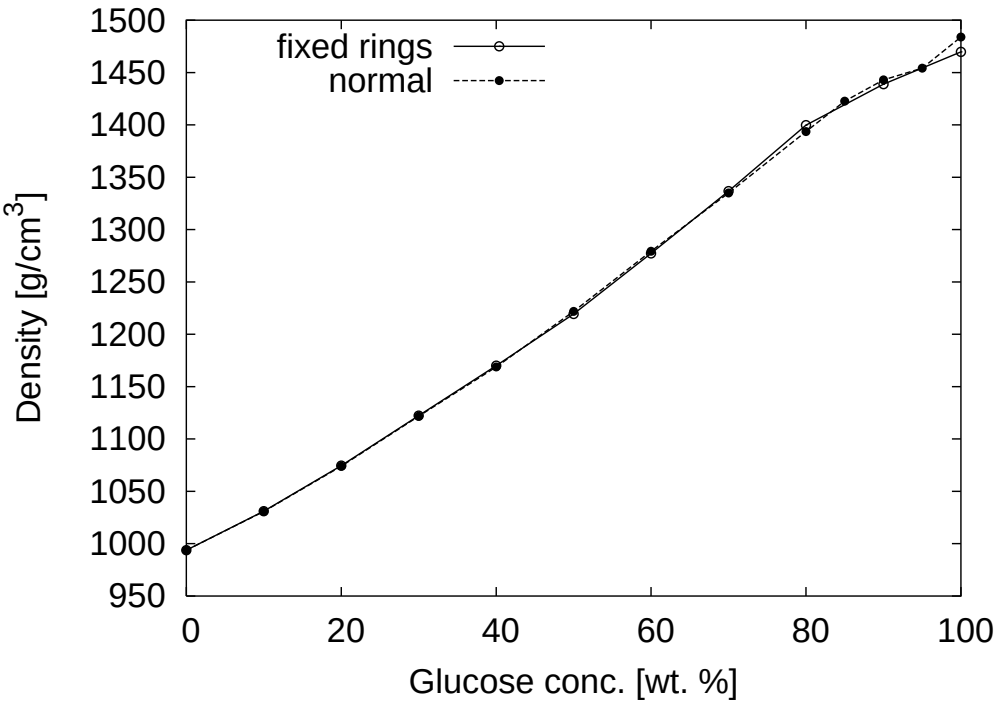

Figure 11: Comparison to simulations with fixed rings: Density of glucose-water mixtures at $T = 310$ K.

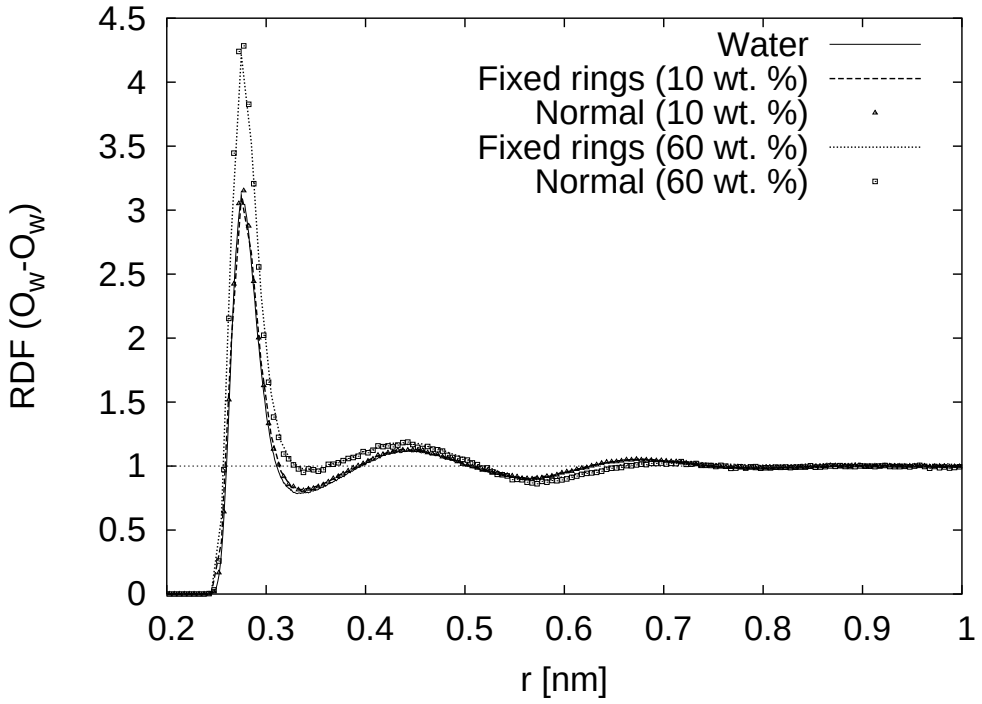

Figure 12: Comparison to simulations with fixed rings: RDF $(O_w - O_w)$ for glucose-water mixtures at $T = 310$ K.

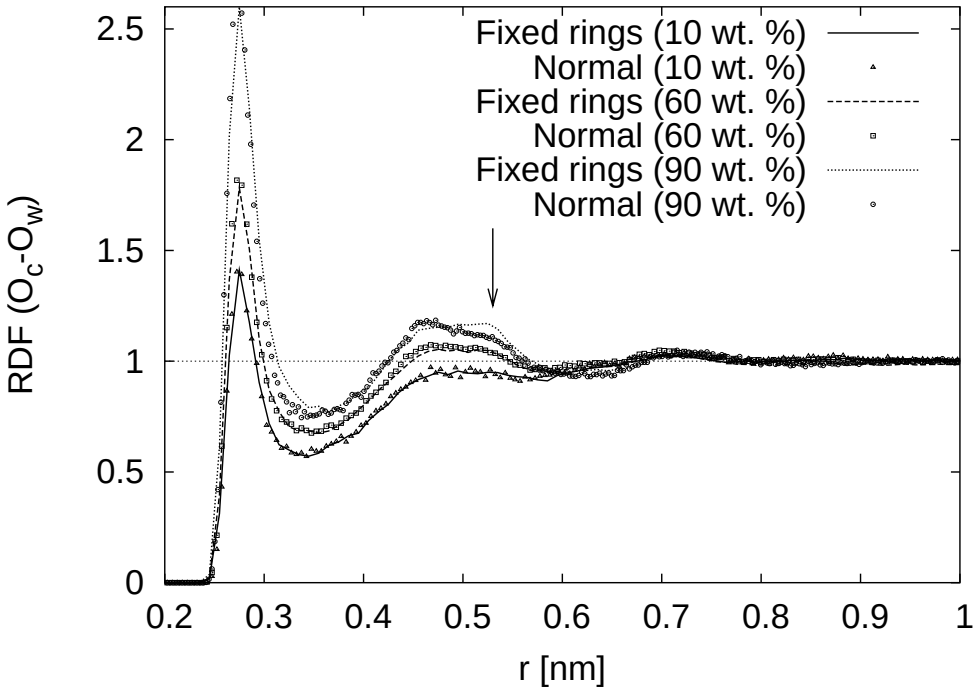

Figure 13: Comparison to simulations with fixed rings: RDF $(O_c - O_w)$ for glucose-water mixtures at $T = 310$ K. The arrow at $r = 0.53$ nm denotes a significant difference for 90 wt.% glucose content.

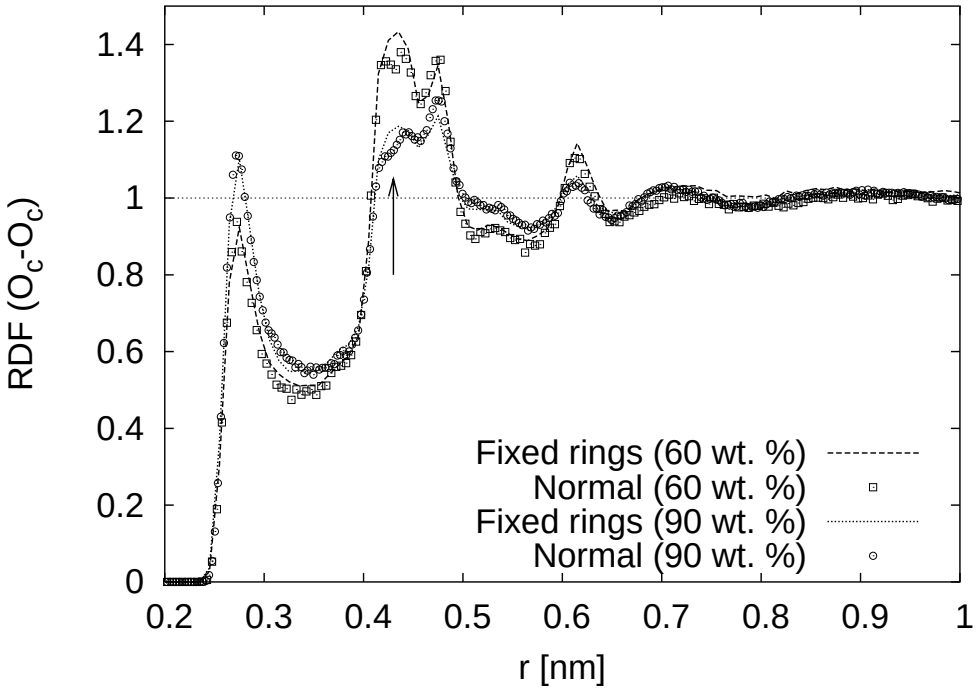

Figure 14: Comparison to simulations with fixed rings: RDF $(O_c - O_c)$. The arrow at $r = 0.43$ nm denotes a significant difference for 90 wt. % glucose.

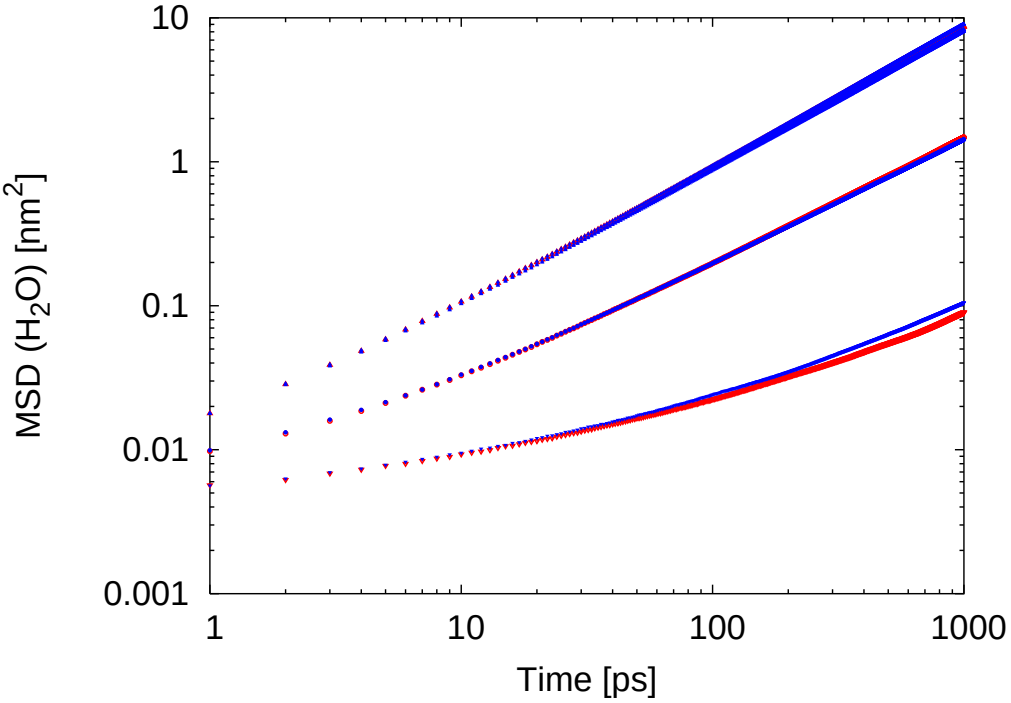

Figure 15: Comparison to simulations with fixed rings: MSD of water. From top to bottom for 40, 70 and 90 wt.% glucose content at $T = 310$ K. Blue symbols are normal simulations and red symbols simulations with fixed rings.

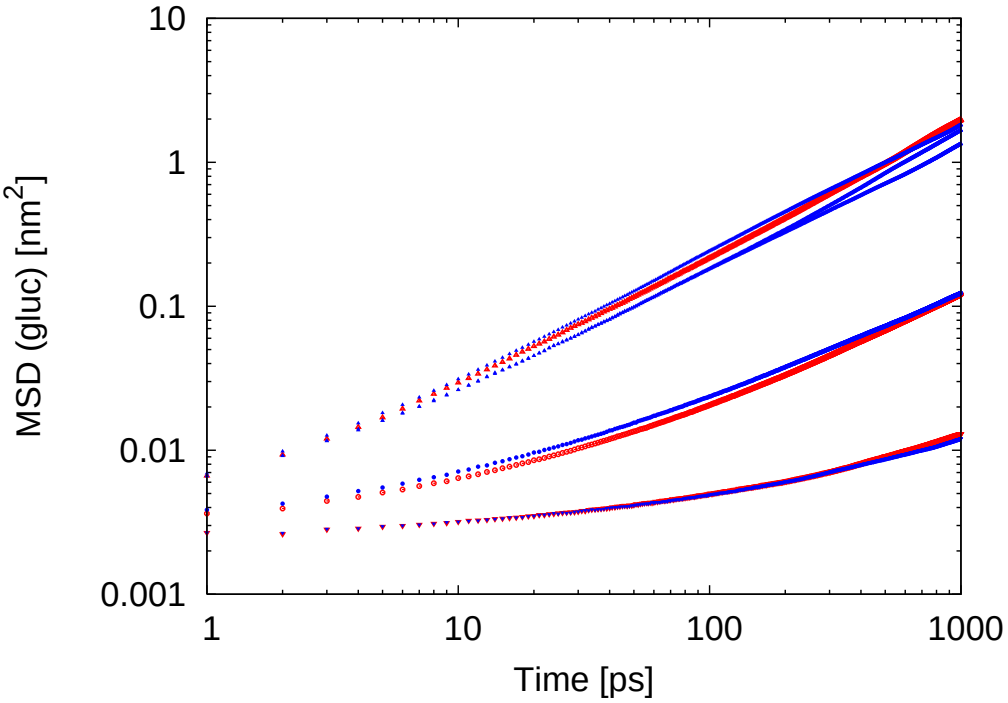

Figure 16: Comparison to simulations with fixed rings: MSD glucose.